Supporting Information:

Attaching onto or Inserting into an Intramolecular Hydrogen Bond: Exploring and Controlling a Chirality-dependent Dilemma for Alcohols

M. Lange, E. Sennert, M. A. Suhm*

E-mail: msuhm@gwdg.de

Theoretical results

Table S1: Applied keywords in ORCA 4.2.1 [S1] and Turbomole 7.3 [S2,S3] for electronic structure optimizations (superscript ES), local energy decompositions (LED), reaction path optimizations (RP) and transition state searches (TS).

Level of approximation	Applied keywords
B3LYP-D3(BJ, abc) / def2-TZVP (ORCA)^{ES}	B3LYP D3BJ def2-TZVP abc grid5 NoFinalGrid UseSym VERYTIGHTSCF TIGHTOPT FREQ
DLPNO-CCSD(T) (ORCA)^{LED}	DLPNO-CCSD(T) TightPNO aug-cc-pVQZ aug-cc-pVQZ/C TightSCF LED
B97-3c-D3(BJ, abc) / def2-TZVP (TURBOMOLE)^{RP}	b973c def2-TZVP grid m5 disp3 bj abc ri
B97-3c-D3(BJ, abc) / def2-mTZVP (TURBOMOLE)^{TS}	b973c def2-mTZVP grid m5 disp3 bj abc ri itrvec 1
B3LYP-D3(BJ, abc) / def2-TZVP (ORCA)^{TS}	B3LYP D3BJ def2-TZVP abc grid5 NoFinalGrid UseSym OptTS VERYTIGHTSCF TIGHTOPT FREQ

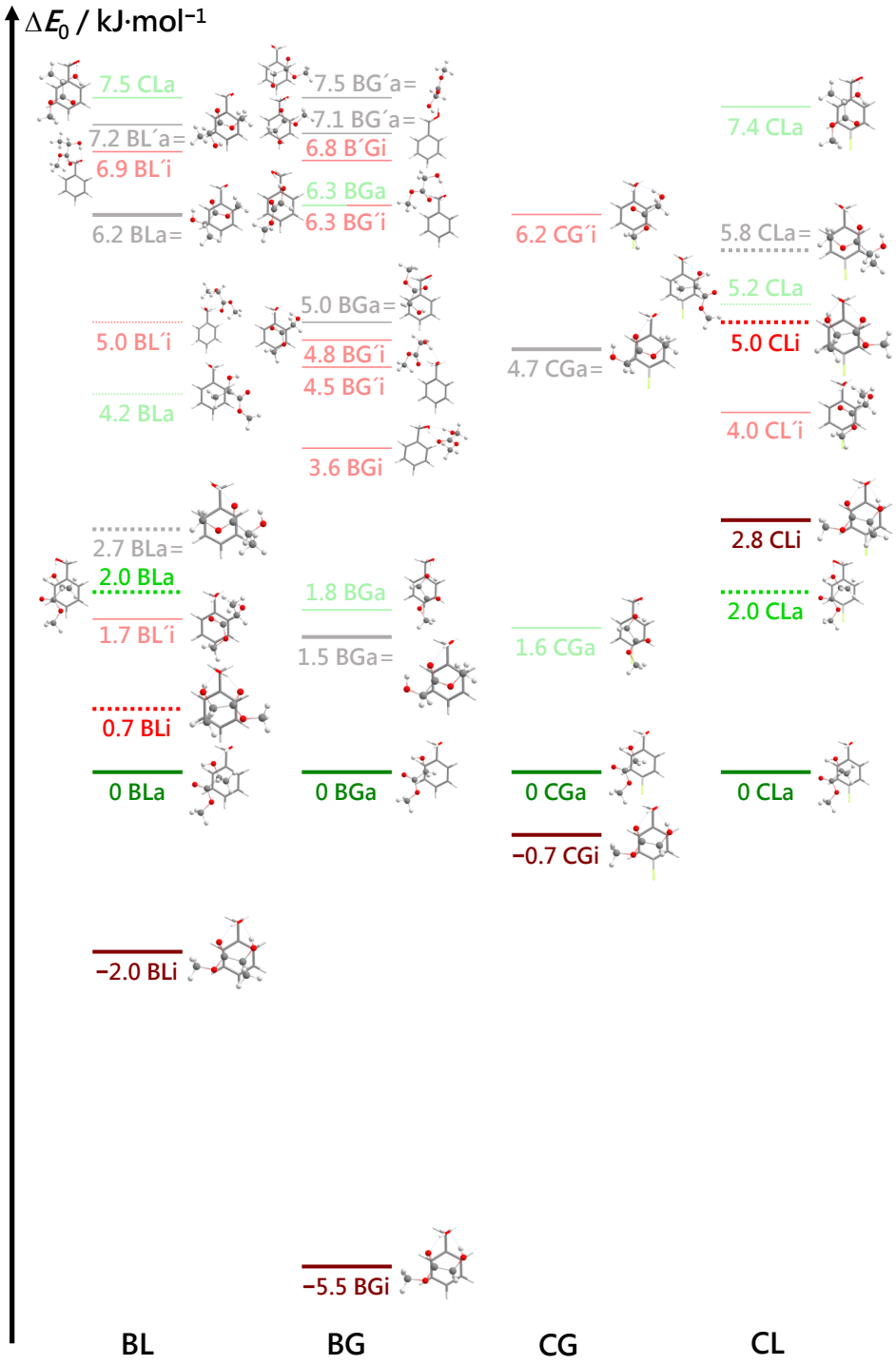

Fig. S1: Optimized structures of the four systems BL, BG, CG and CL and their vibrational zero point-corrected energy differences up to (at most) 8 kJ·mol^{-1} above the respective most stable associated structure, which was chosen as reference point. Solid lines indicate hom structures in which the (*S*)-(−)-lactate induces a *gauche*(−) conformation in the alcohol, whereas het structures are marked with dashed lines. The lines do not imply structural similarity but rather best-in-class property. In structures that contain a prime in their name, the ester conformation or coordination deviates from the most stable structures (with the exception of 6.8 B'Gi, where the alcohol conformation deviates from the usually present *gauche* conformation). Associated structures with a hydrogen bond between the alcohol and the carbonyl oxygen are denoted by =.

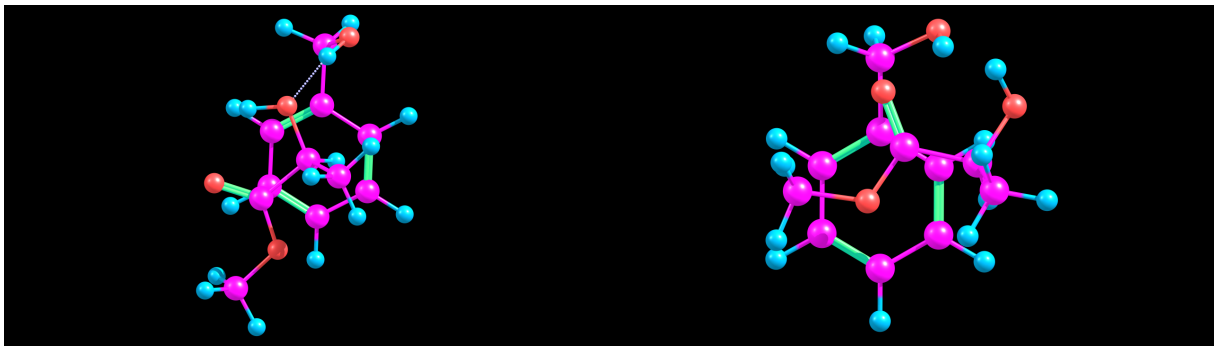

(a) **(b)** 11.2 kJ·mol^{-1}

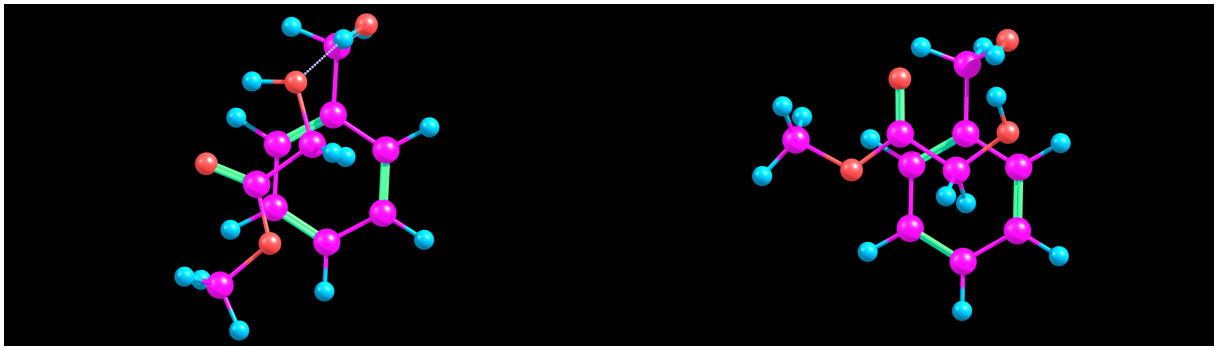

(c) **(d)** 6.6 kJ·mol^{-1}

(e) **(f)** 14.8 kJ·mol^{-1}

(g) **(h)** 13.6 kJ·mol^{-1}

Fig. S2: Left column: animated interconversion paths between the most stable associated complex and the most stable inserted complex for the four systems BL (a), BG (c), CL (e) and CG (g). Right column: transition states of the respective interconversion paths for the four systems BL (b), BG (d), CL (f), CG (h) and their vibrational zero point-corrected barrier heights, as viewed from the associated complex.

Table S2: Performance of the uniformly scaled harmonic wavenumber prediction $\tilde{\nu}_{\mathrm{calc}}$ for the experimental bands assigned in this work (upper part) and in previous investigations of alcohol(phenol) - hydroxyester complexes (lower part, P=phenol, M=methanol, N=(*S*)-2-naphthyl-1-ethanol) as well as the absolute values for the experimental and scaled harmonic band position and the calculated IR band strength.

label this work	**mode**	$\tilde{\nu}_{\mathrm{exp}}$ **/cm^{-1}**	$0.97{\cdot}\tilde{\nu}_{\mathrm{calc}}$ **/cm^{-1}**	**calc. IR band strength /(km/mol)**	$(0.97{\cdot}\tilde{\nu}_{\mathrm{calc}} - \tilde{\nu}_{\mathrm{exp}})$ **/cm^{-1}**
BLa	OH_B	3503	3496	406	–7
BLi	OH_s	3461	3461	78	0
BGi	OH_{as}	3497	3493	609	–4
BGi	OH_s	3453	3449	82	–4
CLa	OH_C	3497	3492	398	–5
CGa	OH_C	3509	3505	363	–4
CGi	OH_{as}	3498	3495	591	–3
CGi	OH_s	3452	3451	82	–1
system	**label (mode)**				
PL[S4]	i (OH_P)	3382	3379	634	–3
PL[S4]	i (OH_L)	3516	3522	561	+6
PL[S4]	a (OH_P)	3453	3462	521	+9
PL[S4]	a (OH_L)	3530	3574	65	+44
NL[S5]	$SR_{1,A}$ (OH_N)	3490	3489	460	–1
NL[S5]	$SR_{1,A}$ (OH_L)	3525	3550	70	+25
NG[S5]	(OH_N)	3501	3500	410	–1
NG[S5]	(OH_G)	3525	3552	60	+27
ML[S6]	1-Ia (OH_M)	3518	3496	728	–22
ML[S6]	1-Ib (OH_L)	3413	3396	330	–17
MG[S6]	0-Ia (OH_M)	3537	3512	658	–25
MG[S6]	0-Ib (OH_G)	3413	3383	454	–30

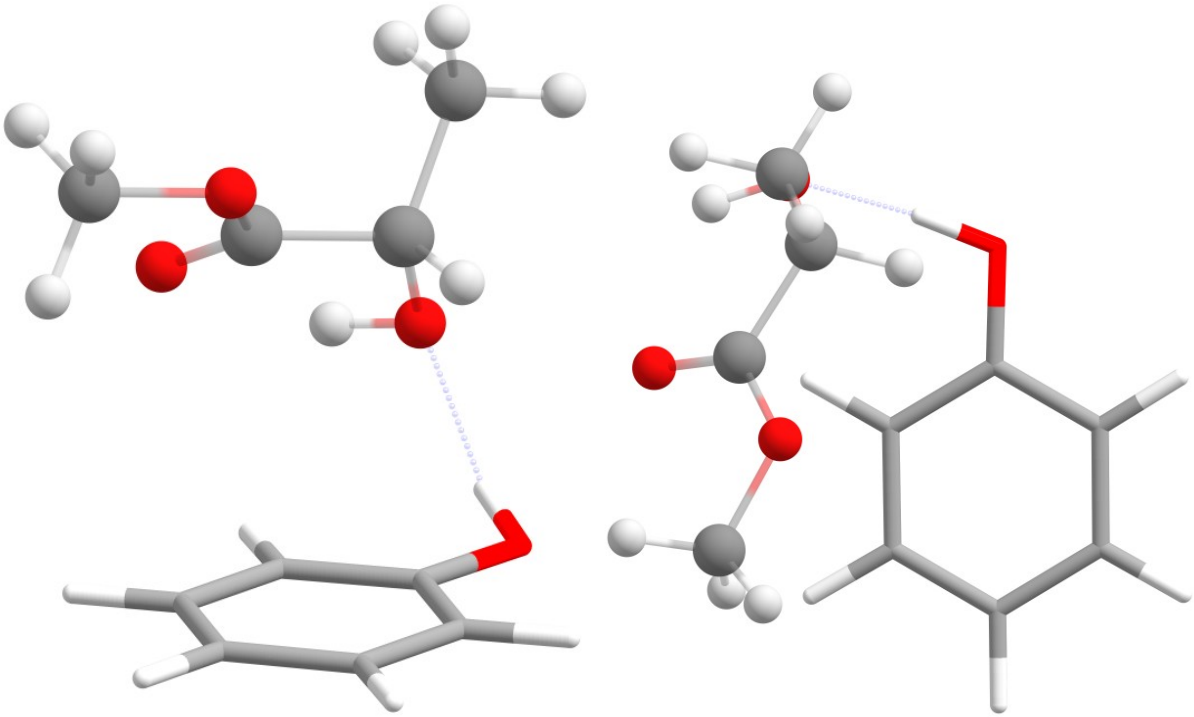

Fig. S3: Optimized structure of the associated PL dimer (a) which was analyzed with regard to the performance of the uniformly scaled B3LYP-D3 method.

Experimental results

Table S3: Roughly estimated relative abundances of all species that can be observed in the BL spectra, determined from the ratio of the calculated intensities (IR: band strengths, Raman: scattering cross sections) and the experimental band integrals. The abundance of B was normalized to 1. [a] It was assumed that all LL bands are caused by a single L dimer. The calculated IR band strength (1040 km/mol) was therefore spread over all individual contributions based on the ratio of the experimental band integrals from a pure L spectrum. Furthermore, only one third of the integral values determined from the mixed BL spectrum were used to calculate the abundances in these cases, in order to allow for possible spectral overlaps with other species. [b] In the IR spectrum, the BB band at 3514 cm^{-1} probably overlaps with an additional LL band at 3515 cm^{-1}. To take this into account, the integral of this LL band was estimated from the visible LL bands and the integral ratio from the pure L spectrum. One third of the value obtained was subtracted from the BB 3514 integral before the abundance was calculated. The uncertainty of this procedure is indicated by specifying the BB 3514 abundance as an upper limit.

IR/Raman	Label	Calculated IR band strength (km/mol)	Abundance
IR	B 3647	21	1
IR	BB' 3598	406	0.01
IR	BB 3582	124	0.08
IR	L 3565	83	0.42
IR	LL 3543	155[a]	<0.01
IR	LL 3529	185[a]	0.01
IR	BB 3514	239	<0.04[b]
IR	BLa 3503	406	0.07
IR	LL 3496	185[a]	0.01
		Raman scattering cross section / (10^{-34} m^2/sr)	
Raman	B 3647	0.61	1
Raman	BB' 3594	2.53	<0.01
Raman	BB 3582	0.74	0.07
Raman	L 3565	0.46	1.60
Raman	BB 3514	0.75	0.19
Raman	BLa 3503	0.80	0.49
Raman	BLi 3461	1.35	0.15

Table S4: Roughly estimated relative abundances of all species that can be observed in the BG spectra, determined from the ratio of the calculated intensities (IR: band strengths, Raman: scattering cross sections) and the experimental band integrals. The abundance of B was normalized to 1. [a] It is unclear which GG structure causes the band at 3547 cm^{-1}. However, the integral ratio of GG 3547 and GG 3512 fits very well with that in pure G spectra. The same abundance is therefore assumed for both bands. [b] In the IR spectrum, the GG band at 3512 cm^{-1} probably overlaps with the BB band at 3514 cm^{-1}. It is known from the mixed BL spectrum as well as pure B spectra that the BB bands at 3514 cm^{-1} and 3582 cm^{-1} have a very similar intensity. To calculate the abundance of GG 3512 adjusted for the overlap, half of the BB 3582 integral was subtracted from the GG 3512 integral. The uncertainty of this procedure is indicated by specifying the GG 3512 abundance as an upper limit.

IR/Raman	**Label**	**Calculated IR band strength (km/mol)**	**Abundance**
IR	B 3647	21	1
IR	BB' 3598	406	0.01
IR	BB 3582	124	0.07
IR	G 3570	74	0.70
IR	GG 3547		<0.03[a]
IR	GG 3512	987	<0.03[b]
IR	BGi 3497	609	0.03
		Raman scattering cross section / (10^{-34} m^2/sr)	
Raman	B 3647	0.61	1
Raman	BB' 3594	2.53	0.01
Raman	BB 3582	0.74	0.07
Raman	G 3570	0.42	1.20
Raman	BB 3514	0.75	0.16
Raman	GG 3496	2.31	0.02
Raman	BGi 3453	1.05	0.22

Table S5: Roughly estimated relative abundances of all species that can be observed in the CL spectra, determined from the ratio of the calculated intensities (IR: band strengths, Raman: scattering cross sections) and the experimental band integrals. The abundance of C was normalized to 1.

IR/Raman	Label	Calculated IR band strength (km/mol)	Abundance
IR	C 3648	23	1
IR	CC 3576	138	0.07
IR	L 3565	83	0.23
IR	CC 3507	242	0.05
IR	CLa 3497	398	0.04
		Raman scattering cross section / (10^{-34} m^2/sr)	
Raman	C 3648	0.63	1
Raman	CC 3576	0.79	0.05
Raman	L 3565	0.46	1.03
Raman	CC 3507	0.75	0.10
Raman	CLa 3497	0.90	0.27

Table S6: Roughly estimated relative abundances of all species that can be observed in the CG spectra, determined from the ratio of the calculated intensities (IR: band strengths, Raman: scattering cross sections) and the experimental band integrals. The abundance of C was normalized to 1. [a] In order to be able to determine abundances despite the overlap of CC 3576 and G 3570 as well as GG 3512 and CGa 3509, the entire integral over both bands was first calculated in both cases. It was then distributed among the two species in a ratio of 1:2 (CC 3576:G 3570, GG 3512: CGa3509). [b] It is unclear which GG structure causes the band at 3547 cm^{-1}. However, the integral ratio of GG 3547 and GG 3512 fits very well with that in pure G spectra. The same abundance is therefore assumed for both bands. [c] In both the IR and Raman spectrum, the CGa band at 3509 cm^{-1} probably overlaps with the CC band at 3507 cm^{-1}. It is known from the mixed CL spectrum as well as pure C spectra that the CC bands at 3507 cm^{-1} and 3576 cm^{-1} have a very similar intensity. To calculate the abundance of CGa 3509 adjusted for the overlap, half of the CC 3576 integral was subtracted from the CGa 3509 integral. The uncertainty of this procedure is indicated by specifying the CGa 3509 abundance as an upper limit.

IR/Raman	**Label**	**Calculated IR band strength (km/mol)**	**Abundance**
IR	C 3648	23	1
IR	CC 3576	138	0.15[a]
IR	G 3570	74	0.57[a]
IR	GG 3547		0.02[b]
IR	GG 3512	987	0.02[a]
IR	CGa 3509	363	<0.07[a, c]
IR	CGi 3498	591	0.02
		Raman scattering cross section / (10^{-34} m^2/sr)	
Raman	C 3648	0.63	1
Raman	CC 3576	0.79	0.06
Raman	G 3570	0.42	1.23
Raman	CGa 3509	0.98	<0.28[c]
Raman	GG 3496	2.31	0.04
Raman	CGi 3452	1.24	0.04

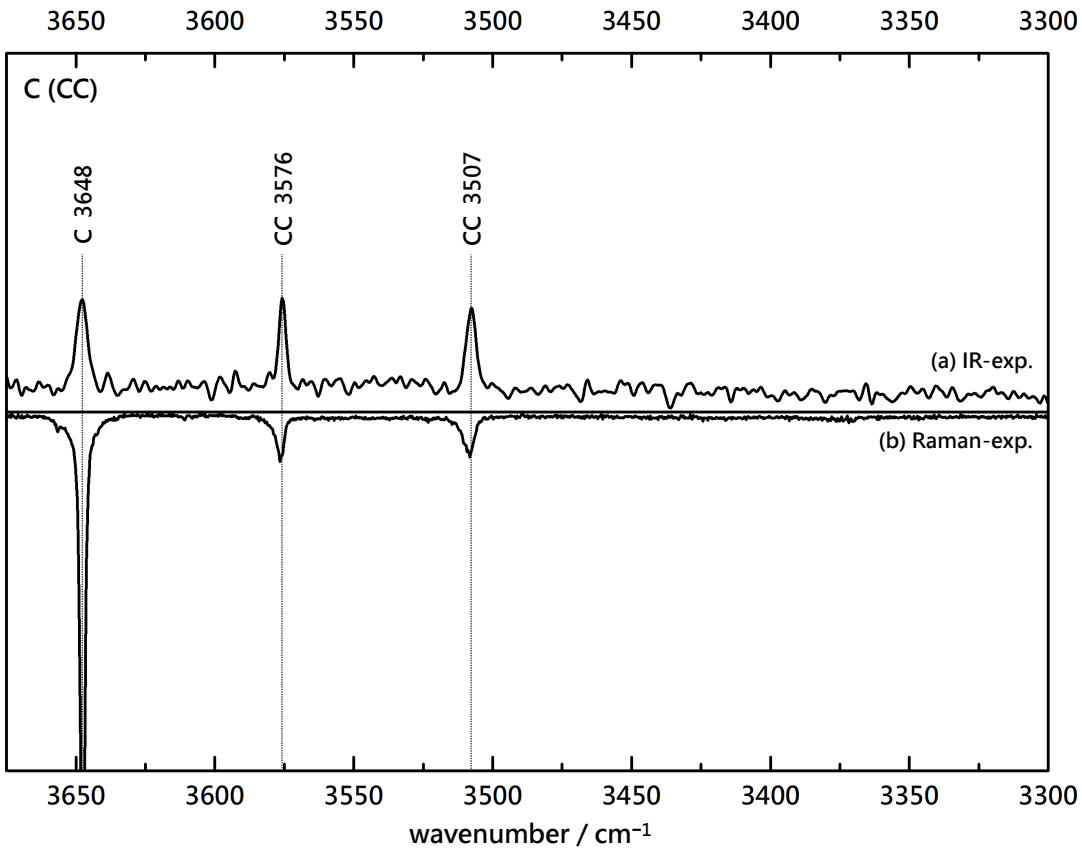

Fig. S4: Comparison of experimental IR (upwards) and Raman (downwards) spectra of (4-)C(hlorobenzyl alcohol) expansions with He. Dotted lines represent contributions from monomer C and dimer CC as marked with their wavenumbers.

References

(S1) Neese, F. Software update: the ORCA program system, version 4.0. *Wiley Interdiscip. Rev. Comput. Mol. Sci.* **2018**, *8*, e1327.

(S2) TURBOMOLE V7.3 2018, a development of University of Karlsruhe and Forschungszentrum Karlsruhe GmbH, 1989-2007, TURBOMOLE GmbH, since 2007; available from `http://www.turbomole.com`.

(S3) Furche, F.; Ahlrichs, R.; Hättig, C.; Klopper, W.; Sierka, M.; Weigend, F. Turbomole. *Wiley Interdiscip. Rev. Comput. Mol. Sci.* **2014**, *4*, 91–100.

(S4) Hong, A.; Moon, C. J.; Jang, H.; Min, A.; Choi, M. Y.; Heo, J.; Kim, N. J. Isomer-Specific Induced Circular Dichroism Spectroscopy of Jet-Cooled Phenol Complexes with (–)-Methyl l-Lactate. *J. Phys. Chem. Lett.* **2018**, *9*, 476–480.

(S5) Seurre, N.; Le Barbu-Debus, K.; Lahmani, F.; Zehnacker, A.; Borho, N.; Suhm, M. A. Chiral recognition between lactic acid derivatives and an aromatic alcohol in a supersonic expansion: electronic and vibrational spectroscopy. *Phys. Chem. Chem. Phys.* **2006**, *8*, 1007–1016.

(S6) Borho, N.; Suhm, M. A.; Le Barbu-Debus, K.; Zehnacker, A. Intra- vs. intermolecular hydrogen bonding: dimers of alpha-hydroxyesters with methanol. *Phys. Chem. Chem. Phys.* **2006**, *8*, 4449–4460.